Sea Level Rise Learning Scenarios for Adaptive Decision-Making Based on IPCC AR6

Vanessa Völz, Jochen Hinkel

Earth's Future

RESEARCH ARTICLE
10.1029/2023EF003662

Sea Level Rise Learning Scenarios for Adaptive Decision-Making Based on IPCC AR6

Vanessa Völz[1,2] and **Jochen Hinkel**[1,2]

[1]Thaer-Institute of Agricultural and Horticultural Sciences, Humboldt-Universität zu Berlin, Berlin, Germany, [2]Global Climate Forum, Berlin, Germany

Key Points:

- We show how climate learning scenarios can be applied for improving and justifying investments in flexible long-lasting infrastructure
- We develop sea level rise learning scenarios based on Intergovernmental Panel on Climate Change sixth Assessment Report using a novel method termed direct fit
- Our new method reduces the average deviation of learning scenarios from the original data by 83% compared to standard methods

Supporting Information:

Supporting Information may be found in the online version of this article.

Correspondence to:

V. Völz,
vanessa.voelz@globalclimateforum.org

Citation:

Völz, V., & Hinkel, J. (2023). Sea level rise learning scenarios for adaptive decision-making based on IPCC AR6. *Earth's Future*, *11*, e2023EF003662. https://doi.org/10.1029/2023EF003662

Received 13 MAR 2023
Accepted 30 AUG 2023

Author Contributions:

Conceptualization: Vanessa Völz, Jochen Hinkel
Data curation: Vanessa Völz, Jochen Hinkel
Formal analysis: Vanessa Völz
Funding acquisition: Jochen Hinkel
Investigation: Vanessa Völz
Methodology: Vanessa Völz
Project Administration: Jochen Hinkel
Resources: Vanessa Völz, Jochen Hinkel
Software: Vanessa Völz, Jochen Hinkel
Supervision: Jochen Hinkel
Validation: Vanessa Völz, Jochen Hinkel

Abstract Adaptation decision-scientists increasingly use real-option analysis to consider the value of learning about future climate variable development in adaptation decisions. Toward this end learning scenarios are needed, which are scenarios that provide information on future variable values seen not only from today (as static scenarios), but also seen from future moments in time. Decision-scientists generally develop learning scenarios themselves, mostly through time-independent (stationary) or highly simplified methods. The climate learning scenarios thus attained generally only poorly represent the uncertainties of state-of-the-art climate science and thus may lead to biased decisions. This paper first motivates the need for learning scenarios by providing a simple example to illustrate characteristics and benefits of learning scenarios. Next, we analyze how well learning scenarios represent climate uncertainties in the context of sea level rise and present a novel method called direct fit to generate climate learning scenarios that outperforms existing methods. This is illustrated by quantifying the difference of the sea level rise learning scenarios created with both methods to the original underlying scenario. The direct fit method is based on pointwise probability distributions, for example, boxplots, and hence can be applied to static scenarios as well as ensemble trajectories. Furthermore, the direct fit method offers a much simpler process for generating learning scenarios from static or "ordinary" climate scenarios.

Plain Language Summary Many climate change adaptation decisions require large investments in infrastructure (e.g., dikes), while at the same time future projections about critical variables (e.g., sea level rise) are highly uncertain. Decision-scientists address these challenges with methods based on flexibility and staged decision-making. For example, a coastal decision-maker could implement a dike with a wider foundation, and, if necessary, upgrade the dike height in the future. The decision-maker will learn by observing future sea level rise if higher dike protection levels are actually necessary in the future. In order to assess whether it is economically beneficial to wait for future learning through observations, and thus to justify additional expenses for flexible infrastructure investments, learning scenarios are required. Learning scenarios provide projections of critical variables seen from today and from future moments in time. For example, learning scenarios of sea level rise contain sea level rise projections seen from 2050 onward, depending on a certain amount of sea level rise observed until 2050. In this paper, we provide a simple example to illustrate coastal decision-making with a learning scenario, propose a new method to generate learning scenarios, and apply this method to generate sea level rise learning scenarios.

1. Introduction

Climate change adaptation decision-making is an interdisciplinary research field that requires close collaboration between climate science and decision science in order to adequately support decision-making. The kind of climate information needed for a specific adaptation decision is thereby determined by the decision-making method applied, which in turn is determined by the decision context (Helgeson, 2018; Hinkel et al., 2019, 2015; Weaver et al., 2017).

For many long-term climate change adaptation decisions the context is shaped by two characteristics. On the one hand, the portfolio of necessary adaptation actions includes large investments in infrastructure, which exhibit long lead and life times, specifically in the water sector (Cooley et al., 2022). For example, dikes exhibit lead times of 5–25 years and life times above 30 years (Climate-ADAPT, 2016). On the other hand, future projections about critical climate variables are highly uncertain due to, amongst others, future greenhouse gas emissions and a poorly constrained climate sensitivity. For example, sea levels in 2100 could range between 28 and 101 cm

Visualization: Vanessa Völz, Jochen Hinkel
Writing – original draft: Vanessa Völz, Jochen Hinkel
Writing – review & editing: Vanessa Völz, Jochen Hinkel

within a 66% likely range across the spectrum of emission pathways considered in the sixth Assessment Report (AR6) of the Intergovernmental Panel on Climate Change (IPCC) (Fox-Kemper et al., 2021). Against this background, it is challenging for public authorities to design long-lasting infrastructure and to justify such expensive investments.

One set of decision-making methods that is considered specifically suitable for contexts with large infrastructure investments and high uncertainties are so-called adaptive decision-making methods (Oppenheimer et al., 2019). These methods emphasize the design of flexible measures and infrastructure, the postponement of decisions and/or staged decision-making, thereby taking into account that learning through observing future climate variables will reduce climate uncertainty (New et al., 2022).

Various adaptive decision-making methods exist, an emerging one of them being real-option analysis. Real-option analysis methods identify optimal adaptation decision rules with respect to probabilistic information about future development of climate variables (Wreford et al., 2020). Similar to real-option analysis, more broadly defined dynamic planning methods use control theory to optimize adaptation decision rules over time (Herman et al., 2020). Note that standard real-option analysis can only be applied to climate scenarios that incorporate probabilistic information, for example, only within one SSP scenario (Kwakkel, 2020). To develop decision rules that consider multiple SSP scenarios, methods such as robust decision-making and dynamic adaptive pathways planning need to be applied on the output of ROA methods. For an example, see Lawrence et al. (2019) and van der Pol et al. (2021). Other prominent adaptive decision-making methods are adaptive planning (Walker et al., 2001), adaptation pathway analysis (Haasnoot et al., 2012), and dynamic adaptive policy pathways (Haasnoot et al., 2013). Adaptive planning generates a basic plan which is updated over time once new information is available (Walker et al., 2001). Adaptation pathway analysis explores different sequences of adaptation policies under alternative external factors changing over time (Haasnoot et al., 2012). Visualizing the different pathways and transitions between them yields a so-called adaptation pathway map. Dynamic adaptive policy pathways extend adaptation pathway analysis with a framework for monitoring climate variables (signposts) over time and triggering adaptation actions if predefined variable thresholds are crossed (Haasnoot et al., 2013).

Here, we focus on real-option analysis and its key advantage to quantify the value of learning in combination with flexible adaptation options (Kind et al., 2018). Thus, real-option analysis can justify whether implementing flexible adaptation options today are worth the extra costs, or if waiting for further knowledge is beneficial (Buurman & Babovic, 2016). This is specifically relevant for public decisions that involve expensive and long-lasting infrastructure, because in such cases, the public sector needs to justify that public money is spent wisely. For example, coastal authorities are confronted with the question of whether it is meaningful to upgrade dikes today or accept temporarily higher flood risks and upgrade in the future when more information about sea level rise is available.

The critical prerequisite for real-option analysis is the availability of probabilistic information of uncertain climate variables that incorporate future learning, for example, projections seen from a future moment in time considering observations until this point in time. We call these projections learning scenarios, as introduced by Hinkel et al. (2019).

Although climate learning scenarios are critical for the economic analysis of adaptation decisions, literature rigorously developing learning scenarios based on the state-of-the-art climate science is scarce. Until now, learning scenarios are not available from authoritative sources such as the IPCC and decision-scientists generally generate learning scenarios about climate variables themselves based on available static scenarios (projections seen from today, see Section 2.1) or historic data. Even though learning scenarios could have a major influence on the outcomes of decisions (see Section 2.2), the generation of climate learning scenarios is to date only superficially linked to climate science (e.g., no sea level rise learning scenarios based on state-of-the-art climate science, i.e., sea level rise projections of AR5 and AR6, exist) (Völz & Hinkel, 2023a). Furthermore, there is hardly any literature that has analyzed how good learning scenarios represent the underlying climate scenarios (Völz & Hinkel, 2023a). See Section 2.3 for a detailed presentation of state-of-the-art climate learning scenarios with a special focus on sea level rise.

We address these research gaps by (a) providing a simple adaptation example to illustrate the characteristics and benefits of learning scenarios for nondecision-scientists, (b) presenting a novel method called direct fit to generate learning scenarios from the static IPCC AR6 sea level rise scenarios as well as the underlying ensemble trajectories, and (c) developing a goodness of fit metric to analyze how good the learning scenarios developed to represent the underlying scenarios.

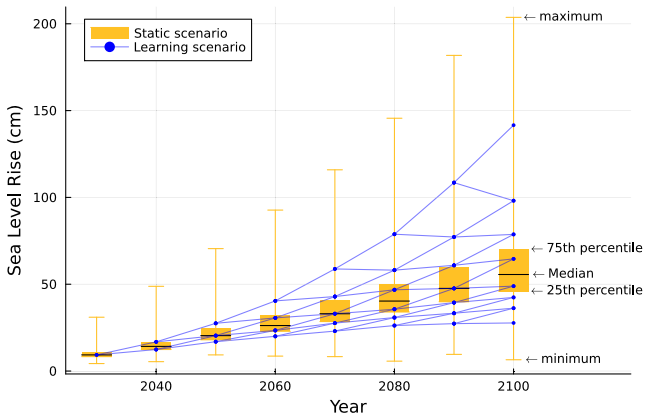

Figure 1. Static sea level rise scenario from Intergovernmental Panel on Climate Change sixth Assessment Report for the shared socioeconomic pathway SSP 2–4.5 plotted as pointwise boxplots (yellow) and a simple learning scenario derived from the static scenario (blue). The yellow boxplots show the minimum value, the 25th percentile value, the median (black line), the 75th percentile value, and the maximum value.

2. State-Of-The-Art

2.1. Static Scenarios Versus Learning Scenarios

Static scenarios provide information on future variable values seen from today, without considering that these estimations can change over time depending on future learning (Völz & Hinkel, 2023a). Well-known examples of static scenarios are the global mean sea level rise projections of the IPCC as shown in Figure 1 (yellow). Dissimilar to standard IPCC sea level rise plots, which plot the data as time-series of given percentile (e.g., median, 17th, and 83rd percentiles), we plot these as sequences of boxplots, because this more accurately represents actual IPCC data. The sea level rise scenarios of AR6 are probability distributions of future sea level rise, given for different moments in time (10 years time steps). Plotting this data as continuous time-series, for example, by connecting the median values of each time step, can lead to misinterpretations. For example, if the median value of sea level rise will be observed in 2040, this does not mean that future sea level rise is going to continue on this median time-series. Plotting the AR6 scenarios as a discrete time series of boxplots emphasizes that the data actually does not contain any information on the connection between time steps.

In contrast to static scenarios, we define learning scenarios as scenarios that provide information on future variable values seen not only from today, but also seen from future moments in time (Hinkel et al., 2019; Völz & Hinkel, 2023a). The information seen from a future moment in time is an updated estimation that is based on learning that occurs until that future moment in time, for example, learning based on observing a climate variable between now and that future moment in time. Please refer to Völz and Hinkel (2023a) for a precise mathematical definition of static scenarios and learning scenarios. In contrast to static scenarios, learning scenarios provide information on the connection between time steps. For example, a sea level rise learning scenario plotted in Figure 1, which has the form of a directed graph and captures a learning effect based on the observed increase of sea level rise every 10 years, provides information on how likely it is to observe the 25th percentile in 2040 and then experience the 50th percentile in 2050.

2.2. A Stylized Decision Using Adaptation Pathways, Learning Scenarios and Real-Option Analysis

We use a simple sea level rise learning scenario and illustrate how it can support a simple adaptive adaptation decision of building a fixed height dike or a flexible dike (i.e., a more expensive dike with the option to upgrade it in the future). Assume a coastal adaptation decision-maker has three adaptation options (two fixed height dikes and one flexible dike) to protect against rising sea levels with respective implementation costs given in Table 1. We illustrate this setting with an adaptation pathway map in Figure 2. Dissimilar to standard adaptation pathway maps, which use a set of alternative and one-dimensional x-axes to represent different static sea level rise scenarios (Haasnoot et al., 2013), we use our two-dimensional learning scenario to represent sea level rise at the bottom of Figure 2. This reveals one crucial advantage of learning scenarios: we not only have information on alternative, disjoint developments of a climate variable seen from today (as offered by static scenarios), but also information on how the different developments of a climate variable are connected with each-other over time.

Table 1
A Simple Example: Adaptation Actions and Implementation Costs

Adaptation action		Costs (Mio $)
A	0.5 m dike	1
B	1 m dike	2
C	0.5 m dike with upgrade option	1.2
A → B	Upgrade dike A to 1 m	2
C → B	Upgrade dike C to 1 m	1

Using the information from the learning scenario, we can now calculate the average adaptation costs occurring in the planning periods 2060 and 2100, depending on the action chosen in 2030. If action A, building a 0.5 m dike, is chosen in 2030, there is a chance of 50% that we will observe low sea level rise in 2060, and we then know that the 0.5 m dike will be effective until 2100. Similarly, there is a 50% chance that we will observe high sea level rise in 2060 and then action A might be insufficient in 2100. Hence, transferring from action A to B in 2060 will be necessary for a risk-averse decision-maker that is not willing to take a 50% chance of being under-protected. Thus, the average adaptation costs when choosing action A in 2030 are: $0.5 \times 1\$ + 0.5 \times (1\$ + 2\$) = 2\$$. Analogously, choosing action B leads to average costs of 2$

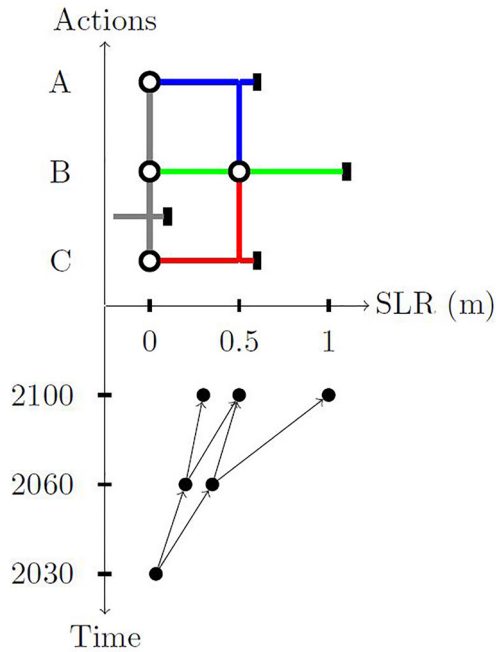

Figure 2. A simple example: adaptation pathway map extended by a sea level rise learning scenario. We choose the probability of transitioning from any node to any of its two next nodes to be 50%. Note that any other combination of probabilities adding up to 1 would in principle be an equally suitable choice, because the value of sea level rise attained at the two next nodes is computed based on these probabilities.

and action C to 1.7$. Hence, this analysis justifies the additional implementation costs for flexible adaptation action C. In this example, we have neglected the issue of discounting in order to keep the illustration clear and simple. In real-world case studies, either private (i.e., risk free rate of return) or social discount rates should be considered because future values are generally worth less than current values due to a range of factors including economic growth, inflation, returns on alternative investments, etc. Furthermore, the discount rate often has significant implications on the outcome of cost-optimal adaptation decisions (Martello & Whittle, 2023).

Whether additional costs for flexible adaptation measures are economically beneficial depends, among others, on the magnitude of future learning. For example, modifying the learning scenario by shifting the medium sea level rise node in 2100 to 0.7 instead of 0.5 m changes the outcome. Switching from action A (or C) to B is always necessary in 2060 for a risk-averse decision-maker, as low sea level rise in 2060 cannot rule out future sea levels above 0.5 m. Then, the average costs for action B are 2$, costs for action A are 3$, and costs for action C are 2.2$. Hence, under the modified learning scenario, building a 1 m dike in 2030 is economically more efficient then a flexible 0.5 m dike.

2.3. Existing Literature of Climate Learning Scenarios and Application to Sea Level Rise

Climate learning scenarios have been developed for a variety of climate-dependent variables such as precipitation (Liu et al., 2018), flood damage (Abadie et al., 2017), sea level rise (Gersonius et al., 2012), water supply (Erfani et al., 2018), river discharge (Kind et al., 2018), climate damages (Bauer et al., 2023; Daniel et al., 2019) and soil fertility (Schou et al., 2015). The majority of these developments thereby apply stationary stochastic processes based on the method of Cox et al. (1979) (Abadie et al., 2017; Gersonius et al., 2013, 2012, K. Kim et al., 2017; M.-J. Kim et al., 2019; Kontogianni et al., 2014; Liu et al., 2018; Oh et al., 2018; Park et al., 2013; Ryu et al., 2018). This method consists in fitting a stationary Geometric Brownian motion to a historic climate variable trajectory and then using this to construct a learning scenario in the form of a graph. A few publications generate climate learning scenarios based on simple, ad-hoc assumptions such that uncertainty is fully reduced at some future point in time (Bruin & Ansink, 2011; Hino & Hall, 2017; Jeuland & Whittington, 2014; Schou et al., 2015; van der Pol et al., 2015, 2013). Others use simplified physical models to generate climate learning scenarios by rerunning the models with future virtual observations (Guillerminet & Tol, 2008; Guthrie, 2019; Webster et al., 2008). More recently, researchers have been using of Bayesian learning to generate nonstationary climate learning scenarios through updating projections with future virtual observations (Dittes et al., 2018; Fletcher, Strzepek, et al., 2019; Guthrie, 2019; Hui et al., 2018; Webster et al., 2008). Two methods (Dittrich et al., 2019; Fletcher, Lickley, & Strzepek, 2019) generate climate learning scenarios on the basis of nonstationary climate model output given as trajectories. Both analyze ensemble trajectories to determine transition probabilities for precipitation learning scenarios.

In the domain of sea level rise, learning scenarios have rarely been applied and the majority of adaptation decision analyses use static sea level rise scenarios (van der Pol & Hinkel, 2019). Even though recent publications emphasize the option to wait for further knowledge about rising sea levels under appropriate circumstances (Slangen et al., 2022), only very few learning scenarios for sea level rise exist. The few existing sea level rise learning scenarios are generated by random sampling of distribution parameters (Woodward et al., 2014), a stochastic process (Gersonius et al., 2013), updating distribution parameters (Linquiti & Vonortas, 2012), simple physical models (Webster et al., 2008) or ad-hoc assumptions (van der Pol et al., 2013).

All of the applied methods to generate learning scenarios for sea level rise are of rather simple nature and not well-grounded on sea level rise science (Völz & Hinkel, 2023a). For example, the stationary stochastic process assumes a constant growth rate and a constant variance over the whole time horizon (Gersonius et al., 2013),

which is inadequate to represent sea level rise uncertainties as sea level rise does not exhibit constant growth rates nor a constant variance over time. Further, the existing learning scenarios (Gersonius et al., 2013; Linquiti & Vonortas, 2012; van der Pol et al., 2013; Webster et al., 2008; Woodward et al., 2014) do not provide any information on how well the learning scenarios represent the underlying data, and neither AR5 nor AR6 sea level rise projections were used as underlying data (Völz & Hinkel, 2023a). We address these shortcomings by developing nonstationary learning scenarios for sea level rise that are based on IPCC AR6 and further use a metric to provide information on how well the learning scenarios represent the underlying data.

A challenge for generating sea level rise learning scenarios lies in the uncertainty of sea level rise projections due to its generation process, as there is no single integrated model that yields trajectories of rising sea levels. Instead, several separate models for each sea level rise component (e.g., Antarctic ice sheet, Greenland ice sheet, thermal expansion etc.) exist, whereas no probabilities can be assigned to the different models for one component and each model has its own parameter and projection uncertainties. This leads to quantifiable uncertainty within each model and ambiguity between the different models for sea level rise components (Kopp et al., 2022). In AR6, multiple probability distributions for different subsets of component models, called workflows, where developed and combined through a p-box approach within FACTS (Framework for Assessing Changes To Sea level) (Kopp et al., 2023). FACTS considers seven different workflows and uses Monte-Carlo sampling to produce 20,000 ensemble trajectories (time-series) for each workflow. The particular p-box approach in AR6 combines probability distributions of several workflows into one static scenario (see Figure 1) by taking the minimum quantile value of all workflow quantile values below 50%, the mean of all 50% quantile values, and the maximum quantile value of all workflow quantile values above 50%.

The application of state-of-the-art methods to generate learning scenarios for sea level rise is limited due to the characteristics of sea level rise projections. A Bayesian approach similar to Fletcher, Lickley, and Strzepek (2019) would only work for each sea level rise component separately, not for the sum of all components. Generation methods based on analyzing trajectories can only be applied to ensemble trajectories of each workflow, not to the static p-box scenario. So far, no generation methods based on quantile functions, as it would be needed for the static p-box scenario, exist.

The contribution of this paper to the climate and sea level scenario literature is threefold. First, we develop a new nonstationary method called direct fit for the generation of learning scenarios, which is based on a highly flexible and efficient algorithm and can be applied to either static scenarios or ensemble trajectories. Second, we provide a goodness of fit metric that can be used to analyze how well learning scenarios represent the underlying data. Both of these methods can be applied to any probabilistic scenario data. Third, we apply our direct fit method to generate sea level rise learning scenarios based on IPCC AR6 scenarios and ensemble trajectories, and use our metric to prove that the learning scenarios sufficiently represent the underlying data. The resulting sea level learning scenarios can be used by anyone appraising coastal adaptation options and adaptation pathways.

3. Methods

3.1. Direct Fit Method

To generate our direct fit learning scenario, we first define a graph structure and then position the nodes of the graph in accordance with the static scenario in each time step. From here on, we refer to the graph as lattice or scenario lattice.

3.1.1. Step 1: Definition of the Lattice Structure

We first define our lattice structure with a fixed number of nodes for each time step and fixed transition probabilities between horizontal neighboring nodes. We choose a binomial and recombining lattice structure, similar to Cox et al. (1979), meaning that each node of the graph transitions into two other nodes in the consecutive time step and that two vertical neighboring nodes transition to the same node in the consecutive time step. This ensures linear growth in the number of nodes with increasing time steps. In contrast to Cox et al. (1979), our method does not rely on a (stationary) stochastic process. Instead, the scenario lattice is fitted directly onto the static scenario, generating a highly flexible and nonstationary lattice shape without any prior distributional assumptions. We enumerate the lattice nodes in each time period with $\mathcal{L}_t = \left\{ l_t^n, \quad n = 1, \ldots, t \right\}$ for $t = 1, \ldots, T$. Note that our binomial and recombining lattice structure defines the cardinality of nodes in each time step as

$|\mathcal{L}_t| = t$. We set the probability p to move upwards to 0.5, similar to the lattice parameters defined by Jarrow and Rudd (1983). The probability p defines the occurrence probability for each node in the lattice and could be set to any number between 0 and 1, as the node positioning process described in the following Section 3.1.2 adjusts the node positions with respect to p.

3.1.2. Step 2: Positioning of the Lattice Nodes

We position all nodes l_t^n of the scenario lattice in accordance with the respective quantile function $Q_t(q)$ of the underlying static scenario. To do this, we define t vertical intervals in each time step t (according to the number of nodes in each time step) and position each node within one interval. We adjust the position and length of the intervals with respect to the occurrence probability of each node l_t^n and the quantile function $Q_t(q)$. The occurrence probability for each node seen from the first time step is given by the binomial distribution:

$$P\left(l_t^n\right) = \binom{t-1}{n-1} p^{n-1}(1-p)^{t-n}. \tag{1}$$

The binomial distribution is shifted by -1 because the indices of $\mathcal{L}_t$ start with $n = 1$, whereas the binomial distribution formula has to start with $n = 0$. To generate t vertical intervals for the node positions, $t + 1$ interval boundaries are required. To be able to generate $t + 1$ interval boundaries, based on $\mathcal{L}_t$ with cardinality t, we define an artificial node l_t^0 with $P\left(l_t^0\right) = 0$ for each time step. Now we have $t + 1$ nodes that we process to $t + 1$ interval boundaries for each time step. We assign a probability value to each node n by summing over the occurrence probability of all nodes lying vertically below the node n in time t. Hence, the interval boundaries for each vertical interval $\Phi_{n,t}$ are given by:

$$\Phi_{n,t} = \left[\sum_{k=0}^{n-1} P\left(l_t^k\right), \sum_{k=0}^{n} P\left(l_t^k\right)\right] \tag{2}$$

for $n = 1, \ldots, t$ and $t = 1, \ldots, T$. To position the nodes l_t^n within the intervals $\Phi_{n,t}$, we use the quantile value of the arithmetic mean of the intervals with

$$l_t^n = Q_t\left(\overline{\Phi}_{n,t}\right) = Q_t\left(\frac{\sum_{k=0}^{n-1} P\left(l_t^k\right) + \sum_{k=0}^{n} P\left(l_t^k\right)}{2}\right) \tag{3}$$

for $n = 1, \ldots, t$ and $t = 1, \ldots, T$. In case the quantile functions $Q_t(q)$ are only defined for a discrete set of quantiles, $q_1, \ldots, q_m$, we use the quantile from this set with the minimal distance to the mean of the interval boundaries

$$l_t^n = Q_t\left(\underset{q \in q_1, \ldots, q_m}{\operatorname{argmin}} |\overline{\Phi}_{n,t} - q|\right) \tag{4}$$

for $n = 1, \ldots, t$ and $t = 1, \ldots, T$. Note that our binomial and recombining lattice structure together with our node positioning process is suitable for a smooth climatic process without abrupt changes, as it forces two transitions of one node to relatively close values in the consecutive time step. As sea level rise scenarios display a smooth climatic process that increases steadily over time, we assume that the direct fit method is suitable to generate learning scenarios for sea level rise.

3.2. Enhancements of Direct Fit

Here, we present two enhancements of the direct fit lattice to improve the goodness of fit to the underlying static scenario at the cost of an increasing number of nodes, which increases the runtime of the decision framework. Increasing the number of nodes of a lattice potentially improves the goodness of fit because this increases the number of data points that store information about quantile values. These enhanced methods could be useful in settings where more precise learning scenarios are needed, for example, because the normal direct fit method does not exhibit a sufficient goodness of fit, and the decision framework does not face computational restrictions due to the increased number of nodes of the shift or skip enhancement.

3.2.1. Shift

The first enhancement is based on the idea to expand the lattice by doubling the time steps and fitting only the second horizontal half of the lattice to the static scenario. This results in a shift of the lattice to the left by the

number of total time steps T. The lattice then contains $T + 1$ nodes instead of one node in the first time step and $2T + 1$ nodes instead of T nodes in the last time step. To generate the shifted direct fit learning scenario, we simply use the formulation in Section 3.1, set the maximum time step to $2T$ instead of T, and position all nodes before the new first time step $(T + 1)$ at any arbitrary value.

3.2.2. Skip

The second enhancement is based on the observation that the direct fit lattice has a better fit to the static scenario in odd time steps compared to even time steps. In odd time steps, the number of nodes is odd and according to the binomial distribution one node is positioned directly on the median. In even time steps, the nodes are positioned next to the median. This results in a zig-zag course over time. We therefore decide to generate a lattice only with odd numbers of nodes in each time step by skipping all even time steps. This creates a trinomial scenario lattice. Similar to the shift method, we use the formulation in Section 3.1 and set the maximum time step to $2T$. We start to position the first node of the lattice on the median value of the quantile function of the first time step. We position the next two following nodes of the lattice at any arbitrary value. Then, the following three nodes of the lattice are positioned according to their occurrence probability (consider odd and even time steps for the binomial distribution) and the quantile function in the second time step. We alternate like this between positioning one vertical node set on arbitrary values (skipping these nodes) and positioning one vertical node set according to the quantile function, until all lattice nodes are positioned.

3.3. Generating Sea Level Rise Learning Scenarios and Analyzing Goodness of Fit

We generate learning scenarios based on the static p-box scenario and on ensemble trajectories from workflow 1f (Fox-Kemper et al., 2021; Garner et al., 2021a; Garner et al., 2021b) by applying the direct fit method (plus enhancements) and the stationary method of Cox et al. (1979) based on a stochastic process. To apply the direct fit methods onto ensemble trajectories, we calculate pointwise quantile functions based on the trajectories and apply the method on these quantile functions. We choose workflow 1f, as this workflow does not rely on Gaussian Process emulations, which model each point in time independently and thus cannot be interpreted as ensemble trajectories (Edwards et al., 2021; Kopp et al., 2023). Instead, workflow 1f uses AR5 data to model the Antarctic ice sheet and glaciers and a parametric ISMIP6 approach to model the Greenland ice sheet (Kopp et al., 2023). All learning scenarios in this manuscript are developed for the global SSP 2–4.5 scenario under medium confidence. We further provide results for learning scenarios based on SSP 1–1.9 and SSP 5–8.5 in the Supporting Information. A detailed description of our implementation of the method by Cox et al. (1979) can be found in the Supporting Information.

To visualize how good a learning scenario represents the underlying static sea level rise scenario, we conduct a Monte-Carlo analysis to obtain quantile functions per time step for each learning scenario. To do so, we draw 10,000 realizations of sea level rise development by randomly choosing a pathway through the scenario lattice. We then generate a sample set with 10,000 data points for every time step according to the realizations. Based on the sample set in each time step, we can calculate quantile values. We can then compare the quantile functions from the learning scenario to the quantile functions of the AR6 sea level rise scenario.

We further develop a metric to quantify the gap between the learning scenario and the underlying static scenario. We use this metric to analyze the gap seen from today and seen from future moments in time, based on artificial observations. As a metric, we use the Wasserstein distance, which quantifies the distance between two probability distributions, to determine the distance between both quantile functions. Stemming from optimal transportation problems, the Wasserstein distance W_p for two probability densities f and g with cumulative distribution functions F and G is defined as (Kolouri et al., 2017):

$$W_p(f,g) = \left(\int_0^1 |F^{-1}(z) - G^{-1}(z)|^p dz \right)^{\frac{1}{p}}. \tag{5}$$

We will use the one-dimensional case $p = 1$, which is also known as the earth mover's distance (Levina & Bickel, 2001). Considering that the inverse cumulative distribution functions in our case are given as discrete quantile functions, we apply the following Euclidean metric to measure the distance between the learning scenario quantile function $Q_t^L(q)$ and the AR 6 sea level rise quantile function $Q_t(q)$ at time step t and quantile q':

$$d(t,q') = |Q_t(q') - Q_t^L(q')|. \tag{6}$$

We further quantify the gap between the learning scenario and the underlying static scenario with an average distance, called overall earth mover's distance. To do so, we sum earth mover's distances over all quantiles and time steps and divide this sum by the number of quantiles and time steps:

$$d_{Q,Q^L} = \frac{1}{T \times m} \sum_{t=1}^{T} \sum_{q=q_1}^{q_m} d(t,q). \tag{7}$$

Moreover, we compute the average distance for several subsets that contain only a few time steps or quantiles. We compute the earth mover's distance for three time intervals ($\mathcal{T}_1 = [2020, 2050]$, $\mathcal{T}_2 = [2060, 2100]$, $\mathcal{T}_3 = [2110, 2150]$) to analyze the time-dependent fit of the learning scenarios. We further compute the average distance for the subset of quantile values below 5% and above 95% to analyze the fat tails fit.

In addition to the goodness of fit analysis mentioned above, which only analyses the fit as seen from today, we add a goodness of fit analysis as seen from future moments in time, based on artificial observations. This analysis can only be done for learning scenarios based on ensemble trajectories, as we need to analyze the information on the transition between time steps, which trajectories provide by definition, but static scenarios do not contain any information on the transition between time steps (see Section 2.1). To test how well a learning scenario can predict a potential future sea level rise range, given a specific sea level observation at a specific future moment in time, we define observation windows. An observation window is defined by an observation year and a minimum and maximum value of sea level rise observations. We then filter all sea level rise trajectories from the workflow and all Monte-Carlo sampled learning scenario pathways that are lying in this observation window (see Figure 7). Based on these filtered trajectories and filtered learning scenario pathways, we can calculate quantile functions for both sea level projections conditional on the given observation. We then apply the earth mover's distance to quantify the gap between both quantile functions. We consider observation windows at all time steps (2040, 2050, …, 2140) with 20 observation windows in each time step, defined by the quantile values 0%, 5%, …, 95%, 100%. We present average earth mover's distances for three subsets of observation years ($T_1 = [2030, 2050]$, $\mathcal{T}_2 = [2060, 2100]$, $\mathcal{T}_3 = [2110, 2140]$) and the lowest (0%–5%) and highest (95%–100%) observation windows.

4. Results

The sea level rise learning scenarios generated by the direct fit (plus enhancements) methods and the stochastic process method are visualized in Figure 3 for the static p-box scenario and in Figure 4 for the workflow 1f trajectories.

We visualize how good the learning scenarios represent the underlying scenario as seen from today by using the Monte-Carlo analysis described in Section 3.3 and plot the resulting quantile functions as boxplots in Figure 5 for the static p-box scenario and Figure 6 for the workflow 1f trajectories.

Quantifying the gap between the learning scenario quantile functions and the underlying scenarios yields absolute earth mover's distances (Equation 6) for each quantile value and time step, which are plotted as histograms for the static p-box scenario and the workflow 1f trajectories in the Supporting Information. Table 2 presents the average earth mover's distances together with the number of unique nodes for each learning scenario for the static p-box scenario and workflow 1f. The smaller the earth's mover's distance is the less deviation between the learning scenario quantile function and the underlying static scenario exists. In other words, the smaller the earth's mover's distance is, the better the learning scenario mimics the underlying static scenario.

We further analyze how well the learning scenarios based on workflow 1f trajectories represent future sea level rise as seen from future moments in time, based on artificial observations. Figure 7 illustrates how we filter the trajectories and Monte-Carlo sampled learning scenario pathways by one observation window. The resulting quantile functions representing future sea level rise, plotted as boxplots, can then be used to calculate the earth mover's distance.

We present the average earth mover's distances for different learning scenarios and subsets of observation windows in Table 3.

The learning scenario by Cox et al. (1979) based on a stochastic process exhibits a good fit for the last time step (the stochastic process is fitted to the last time step, see Supporting Information S1 for details), but is insufficient

10.1029/2023EF003662

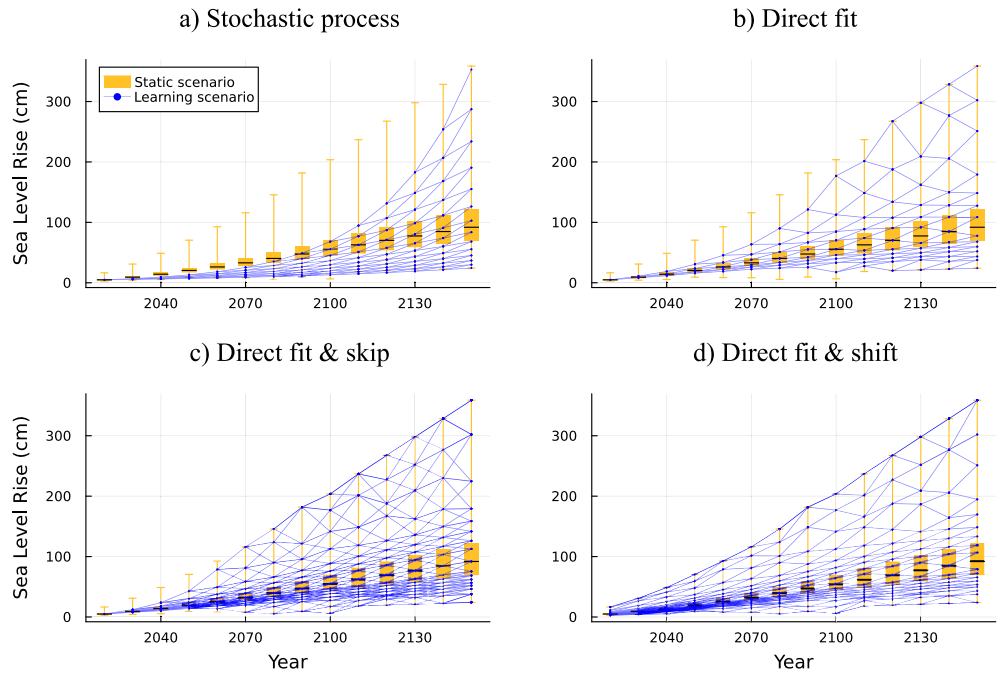

Figure 3. Learning scenarios (blue) based on static p-box SSP 2–4.5 AR6 sea level rise scenario (yellow), which is plotted as pointwise boxplots. Learning scenarios are generated by (a) a stochastic process by Cox et al. (1979), (b) direct fit, (c) direct fit and skip, and (d) direct fit and shift. The boxplots show the minimum value, the 25th percentile value, the median (black line), the 75th percentile value, and the maximum value.

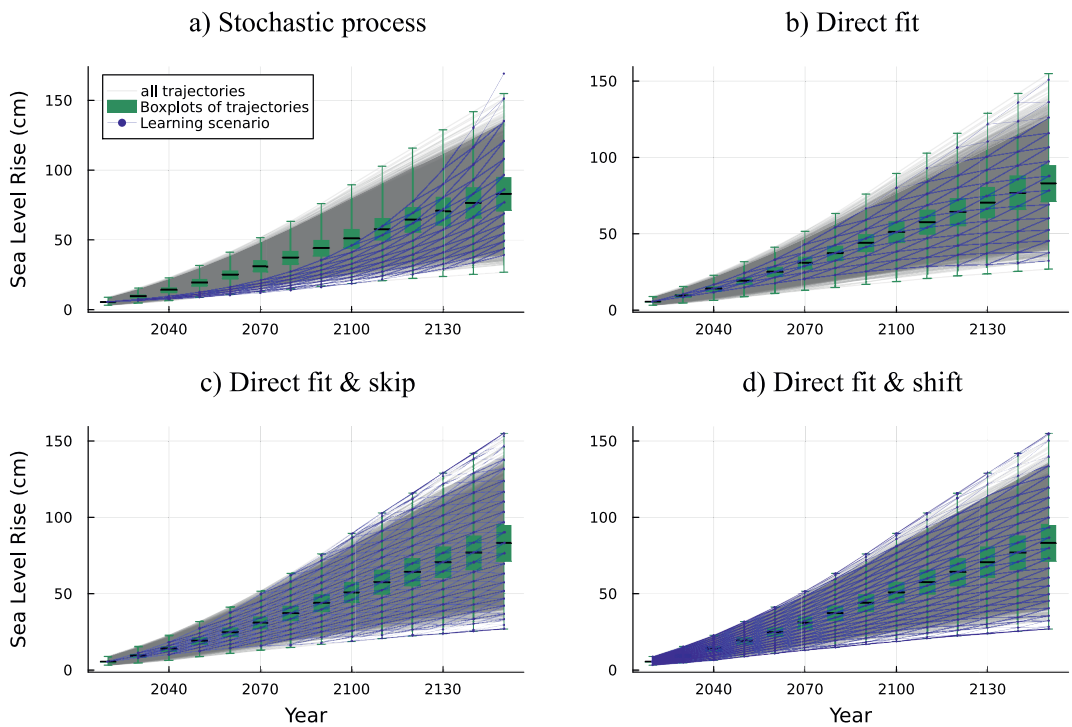

Figure 4. Learning scenarios (blue) based on trajectories of SSP 2–4.5 AR6 sea level rise workflow 1f (gray), which are plotted as pointwise boxplots (green). Learning scenarios are generated by (a) a stochastic process by Cox et al. (1979), (b) direct fit, (c) direct fit and skip, and (d) direct fit and shift. The boxplots show the minimum value, the 25th percentile value, the median (black line), the 75th percentile value, and the maximum value.

10.1029/2023EF003662

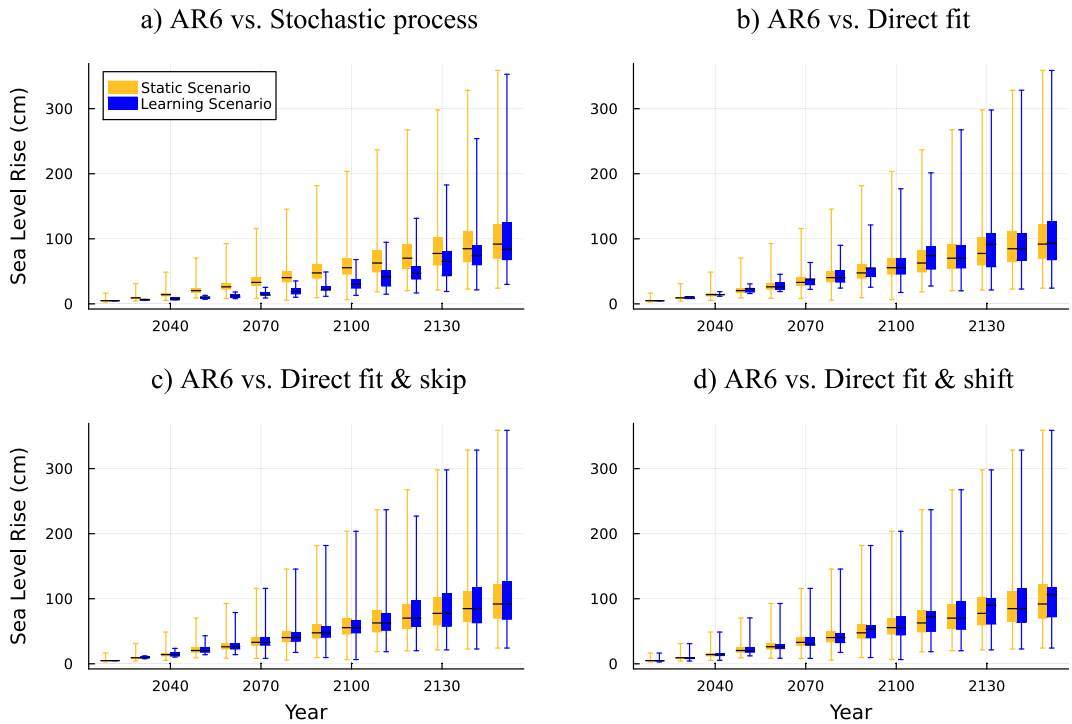

Figure 5. Learning scenario quantile functions (blue) generated through Monte-Carlo analysis of each learning scenario. Learning scenarios are generated by (a) a stochastic process by Cox et al. (1979), (b) direct fit, (c) direct fit and skip, and (d) direct fit and shift. All learning scenarios are based on the static p-box SSP 2–4.5 AR6 sea level rise scenario (yellow). All quantile functions are plotted as pointwise boxplots, which show the minimum value, the 25th percentile value, the median (black line), the 75th percentile value, and the maximum value.

to represent sea level rise in the rest of the time horizon. It clearly shows in the quantile function comparison based on the Monte-Carlo Analysis in Figures 5 and 6, and even in the learning scenario plot in Figures 3 and 4, that the exponential shape of the learning scenario is insufficient to represent sea level rise development. The scenario deviations (18/12 cm on average and often up to 50/30 cm, especially for high end sea level rise, see Table 2 and the histogram figures in the Supporting Information, lead to a severe underestimation of flood risks and are problematic if coastal protection measures are aligned to it. For example, in our adaptation example (Section 2.2), a deviation above 20 cm would clearly lead to highly imprecise adaptation decisions.

Our direct fit method clearly outperforms the stochastic process method for all average distances to the underlying scenario, while having exactly the same number of lattice nodes (Tables 2 and 3). We can reduce the distances at the cost of additional lattice nodes by applying the shift or skip enhancement, whereas the direct fit and shift method with the highest number of nodes clearly outperforms all other methods. The histograms in the Supporting Information show that the direct fit methods rarely exhibits a distance to the underlying scenario greater than 10 cm, which is an acceptable deviation for planning coastal protection measures, for example, dike heights are not planned in increments below 10 cm. Table 3 reveals that the direct fit method applied to workflow 1f trajectories (average deviation below 5 cm) reasonably represents the underlying data seen from future moments in time, based on artificial observations.

The earth mover's distances for time step subsets reveal that the goodness of fit decreases over time within all direct fit learning scenarios (Table 2). The quantile subsets show that all learning scenarios based on the static p-box scenario are considerably better in modeling low sea level rise values than high sea level rise values, whereas this effect is negligible for workflow 1f scenarios.

5. Discussion

Our results show that the stationary method based on a stochastic process, which is often applied to generate climate learning scenarios, is insufficient in the case of sea level rise. The method was originally developed to

10.1029/2023EF003662

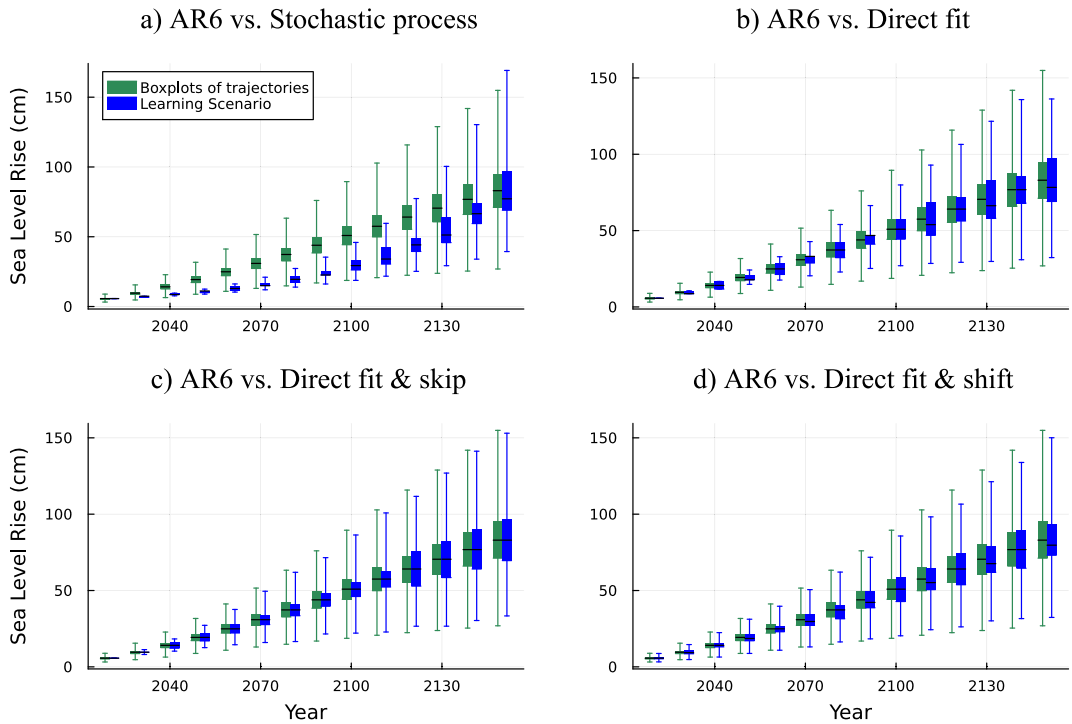

Figure 6. Learning scenario quantile functions (blue) generated through Monte-Carlo analysis of each learning scenario. Learning scenarios are generated by (a) a stochastic process by Cox et al. (1979), (b) direct fit, (c) direct fit and skip, and (d) direct fit and shift. All learning scenarios are based on the trajectories of SSP 2–4.5 AR6 sea level rise workflow 1f (green). All quantile functions are plotted as pointwise boxplots, which show the minimum value, the 25th percentile value, the median (black line), the 75th percentile value, and the maximum value.

model stock price developments by assuming constant growth rates, that is, a stationary Geometric Brownian motion. It should thus not surprise that the constant growth rate assumption is not valid for climate variables such as sea level rise. Recently, Sims et al. (2021) argued that Geometric Brownian motions often fail to represent climate scenarios. We provided evidence for this hypothesis with our quantitative analysis. Furthermore, the method of Cox et al. (1979) was once developed to project economic variable development based on one historic time-series and later adopted by climate adaptation studies to project climatic variables. However, usually not only historic data about physical climate variables exist, instead, detailed scenarios about future climate variable

Table 2
Earth Mover's Distances Between Quantile Functions Stemming From Different Learning Scenarios Compared to the Quantile Function From the Static p-Box SSP 2–4.5 Scenario or the Trajectories of Workflow 1f

			Earth mover's distance (cm)					
Learning scenario	#Nodes	Data	Overall	$t \in \mathcal{T}_1$	$t \in \mathcal{T}_2$	$t \in \mathcal{T}_3$	$q < 5\%$	$q > 95\%$
Stochastic process	105	p-box	17.6	6.4	24.1	20.0	8.6	47.6
		wf 1	12.3	4.4	17.2	13.2	5.7	19.2
Direct fit	105	p-box	3.2	1.6	3.4	4.4	2.8	13.8
		wf 1	1.5	0.8	1.5	2.2	2.5	3.0
Direct fit and skip	196	p-box	2.4	1.3	2.1	3.5	1.3	6.7
		wf 1	1.1	0.6	1.0	1.5	1.6	1.8
Direct fit and shift	287	p-box	1.6	0.4	1.5	2.8	0.7	3.8
		wf 1	0.8	0.2	0.7	1.4	0.7	1.1

Note. Average earth mover's distances (overall), earth mover's distances for several subsets of quantiles and time steps ($\mathcal{T}_1 = [2020, 2050]$, $\mathcal{T}_2 = [2060, 2100]$, $\mathcal{T}_3 = [2110, 2150]$) and the number of nodes (#Nodes) for each learning scenario are provided.

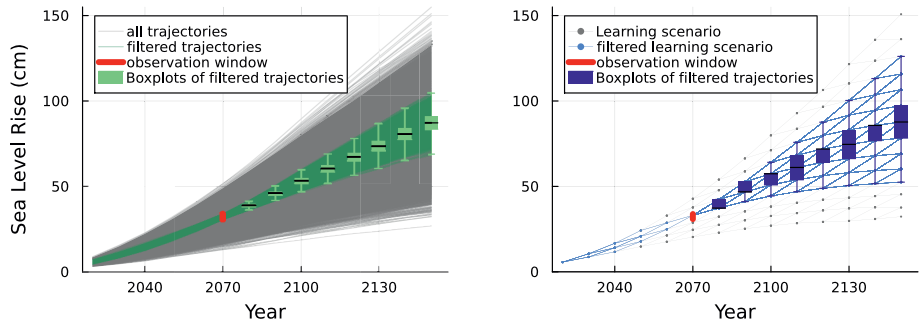

Figure 7. Workflow 1f trajectories (left) and direct fit learning scenario (right) filtered by an observation window. The observation window filters all sea level rise values in 2070 lying between the 50% and 70% quantile value of workflow 1f. Based on the filtered trajectories or on the filtered pathways in the learning scenario, future sea level rise boxplots seen from the observation in 2070 are plotted.

developments based on physical knowledge are often available. Given this knowledge, it is unreasonable to use stationary assumptions based on constant growth rates, instead of using the information from science-based climate scenarios.

We have shown that our direct fit learning scenarios, applied to the IPCC ensemble trajectories, are able to reasonably represent future sea level rise transition behavior between time steps, conditional on future observations, with average deviations below 5 cm (Table 3). This is not obvious, as the direct fit method is exclusively based on quantile functions (calculated from the ensemble trajectories) and hence static probabilistic scenarios, which, by definition, represent sea level rise as a lottery held for each time step separately without transition information. To fill in this information, our method makes assumptions about the transition behavior between different time steps. The assumption on the transition behavior in our model is less restrictive compared to Cox et al. (1979), as all nodes can have flexible positions and no distributional assumptions are made. The predefined assumption of a binomial recombining lattice structure forces the two transitions of one node to relatively close values in the following time step, instead of, for example, jumping to highly deviating quantile values. We have shown with our analysis in Table 3 that this assumption is suitable in the case of sea level rise scenarios, where large abrupt changes in sea level rise are physically impossible and, instead, sea level scenarios rise steadily over time. When applying our method to other climate variables where only static scenarios are available, it is important to check that the underlying climatic process is smooth, that is, does not exhibit massive abrupt changes.

Learning scenarios based on the static p-box scenario allow decision-scientists to consider the ambiguity of sea level rise projections stemming from different component models, whereas learning scenarios based on ensemble trajectories enable a highly precise analysis for one specific component model subset (Tables 2 and 3). The better fit of learning scenarios based on ensemble trajectories can be explained by the availability of any quantile values

Table 3
Earth Mover's Distances Based on Future Observation Windows Between Quantile Functions Stemming From Different Learning Scenarios (Based on Workflow 1f) Compared to the Quantile Function From Trajectories of Workflow 1f (SSP 2–4.5)

	Earth mover's distance (cm)					
Learning scenario	Overall	$t \in \mathcal{T}_1$	$t \in \mathcal{T}_2$	$t \in \mathcal{T}_3$	$q < 5\%$	$q > 95\%$
Stochastic process	16.2	8.1	17.4	16.6	10.2	18.9
Direct fit	4.5	4.8	5.1	3.9	3.9	4.8
Direct fit and skip	4.7	5.8	5.1	3.8	4.6	5.3
Direct fit and shift	2.4	2.0	2.6	2.5	2.0	2.5

Note. We define 20 observation windows in each year of observation through the workflow 1f quantile function, for example, 0%–5% quantile value. We present average earth mover's distances for all observation windows in all learning years (overall), average earth mover's distances for subsets of observation years ($\mathcal{T}_1 = [2030, 2050]$, $\mathcal{T}_2 = [2060, 2100]$, $\mathcal{T}_3 = [2110, 2140]$) and average earth mover's distances for the lowest and highest observation windows.

from the ensemble trajectories, whereas the static p-box scenario only contains 107 quantile values and we need to take the nearest quantile value for the quantile value we actually need in the direct fit method. Theoretically, any quantile value could be generated for the static p-box scenario, but at the moment AR6 output only provides 107 values. This effect can be seen in the learning scenarios, the learning scenarios based on ensemble trajectories are smoother (Figure 4), whereas the learning scenarios based on the stat p-box approach exhibit zig-zag pathways to one of the 107 quantile values (Figure 3).

An advantage of our direct fit method for generating learning scenarios is that it allows a computationally efficient decision analysis, because it creates learning scenarios with a binomial and recombining lattice structure. While the stationary stochastic process method of Cox et al. (1979) and the stationary methods of Bauer et al. (2023) and Daniel et al. (2019) exhibit such a recombining binomial lattice structure, none of the recent nonstationary approaches relying on climate science exhibits a binomial and recombining structure. The latter methods generate either nonrecombining (Erfani et al., 2018; Kind et al., 2018) or non-binomial (Dittrich et al., 2019; Fletcher, Lickley, & Strzepek, 2019; Hui et al., 2018) learning scenarios, which have the advantage of flexible lattice structures that can represent nonexponential and nonsmooth climate variables. Nonrecombining learning scenarios exhibit exponential growth in the number of nodes as the time horizon increases and nonbinomial learning scenarios exhibit a large number of transitions. Both create a computational burden that restricts the number of time steps or learning variables in a decision framework (Herman et al., 2020). The computational efficiency of the direct fit method offers a great opportunity to consider nonstationary learning scenarios for multiple climate and also other (e.g., socioeconomic) variables at the same time (Haasnoot et al., 2018), which has, to our knowledge, not been done yet. However, combining multiple climate variables within one learning scenario can be beneficial, for example, observing changes in the Antarctic snow accumulation can detect a forthcoming collapse of the Antarctic ice sheet, leading to rapid sea level rise, whereas observations of sea levels cannot detect this forthcoming collapse before sea levels actually start to rise rapidly (Scambos et al., 2017).

Further improvements in sea level rise learning scenarios could be gained if climate scientists working on sea level rise projections are aware of learning scenarios and incorporate this in the generation process. For example, the land-ice emulator output of Edwards et al. (2021) cannot be interpreted as ensemble trajectories due to yearly independent emulation; however, the awareness of decision-scientists' demand for ensemble trajectories could be incorporated into the next generation land-ice models and emulators. If land-ice emulators enable yearly dependent emulation, learning scenarios could be fed by new land-ice projections based on additional emulation runs with artificial future sea level observations as input parameters. Another option for improved learning scenario generation methods would be to incorporate a Bayesian approach similar to Fletcher, Lickley, and Strzepek (2019) within the sea level rise component framework (FACTS) for each sea level rise component model (Kopp et al., 2023).

It is important to note that all learning scenarios that we discussed in this paper consider future learning based on observations and not on other ways of scientific knowledge gain such as improvements in numerical models. The latter, however, also contributes to future learning about sea level rise and other climate variables. For example, the understanding of ice sheet processes improved remarkably between the IPCC fourth assessment report in 2007 and the special report in 2019 (Oppenheimer et al., 2019). Another example is the new storyline approach within the IPCC AR6 that determines the potential for a high-end sea level scenario (IPCC, 2021). It is therefore advisable to monitor not only future sea level rise observations and other climate variables, but also scientific advances in the respective field of science.

Finally, the question remains how the direct fit learning scenarios will influence the outcome of a decision framework compared to other learning scenarios. While it is uncontroversial that more precise learning scenarios should be applied within adaptation decisions, the impact on the outcomes of such adaptation decisions needs to be demonstrated on a case by case basis, as this depends not only on the underlying climate data, but also on the kind of adaptation options available, in particular on their lead times, life times, costs and flexibility.

6. Conclusion

Expensive and long-lasting adaptation measures in combination with highly uncertain future developments lead to challenging decision-making problems. In this paper, we provided a simple adaptation decision-making example showing how real-option analysis, based on adaptivity and the consideration of future learning by using

climate learning scenarios, can support such adaptation decisions through providing information on whether it is cheaper to implement more costly flexible adaptation measures or cheaper inflexible ones. The merits of this approach, however, depend on how well the learning scenarios represent the uncertainties in the underlying physical systems and the methods used for generating sea level rise learning scenarios up to now, have not delivered very precise results.

In order to fill this gap, we introduced a novel method called direct fit to generate climate learning scenarios. We have shown that this method has a better fit to underlying state-of-the-art sea level rise scenarios than a commonly used method based on a stochastic process. By analyzing the direct fit learning scenario conditional on future artificial sea level observations, we have shown that the method is able to reasonable represent sea level rise development over time and hence future learning through observations. We recommend that real-option analysis which consider learning about climate uncertainty use the direct fit method rather than stationary methods, if static future scenarios or ensemble trajectories about climate variable development are available, because (a) the shape of the learning scenario is highly flexible to precisely represent climate uncertainties, (b) a small number of nodes ensure computational efficiency, and (c) the generation process is simple. Follow-up case studies could explore the value of learning scenarios within adaptive decision-making methods in comparison to static decision-making methods, for example, cost-benefit analysis.

Conflict of Interest

The authors declare no conflicts of interest relevant to this study.

Data Availability Statement

The IPCC AR 6 sea level rise data sets (Garner et al., 2021a) used in this study are available at https://podaac.jpl.nasa.gov/announcements/2021-08-09-Sea-level-projections-from-the-IPCC-6th-Assessment-Report. The Jupyter manuscript used to generate and analyze the learning scenarios can be accessed via https://zenodo.org/record/8079469 (Völz & Hinkel, 2023b).

Acknowledgments
We would like to thank Tim Hermans for providing valuable information on FACTS and feedback on our method. Vanessa Völz has been funded by the Deutsche Forschungsgemeinschaft (DFG, German Research Foundation) within the Special Priority Program SPP-1889 SeaLevel - project SEASCApe II (Grant 313917492). This publication was supported by PROTECT. This project has received funding from the European Union's Horizon 2020 research and innovation programme under grant agreement No 869304, PROTECT contribution number 73. The article processing charge was funded by the Deutsche Forschungsgemeinschaft (DFG, German Research Foundation)—491192747 and the Open Access Publication Fund of Humboldt-Universität zu Berlin. Open Access funding enabled and organized by Projekt DEAL.

References

Abadie, L. M., de Murieta, E. S., & Galarraga, I. (2017). Investing in adaptation: Flood risk and real option application to Bilbao. *Environmental Modelling & Software*, *95*, 76–89. https://doi.org/10.1016/j.envsoft.2017.03.038

Bauer, A., Proistosescu, C., & Wagner, G. (2023). Carbon dioxide as a risky asset. Available at SSRN 4350865.

Bruin, K. D., & Ansink, E. (2011). Investment in flood protection measures under climate change uncertainty. *Climate Change Economics*, *2*(4), 321–339. https://doi.org/10.1142/s2010007811000334

Buurman, J., & Babovic, V. (2016). Adaptation pathways and real options analysis: An approach to deep uncertainty in climate change adaptation policies. *Policy and Society*, *35*(2), 137–150. https://doi.org/10.1016/j.polsoc.2016.05.002

Climate-ADAPT. (2016). Improved design of dikes and levees. Retrieved from https://climate-adapt.eea.europa.eu/en/metadata/adaptation-options/adaptation-or-improvement-of-dikes-and-dams

Cooley, D. S., Schoeman, L., Bopp, P., Boyd, S., Donner, D., Ghebrehiwet, S.-I., et al. (2022). Oceans and coastal ecosystems and their services. In H.-O. Pörtner, D.C. Roberts, M. Tignor, E. S. Poloczanska, K. Mintenbeck, A. Alegría, et al. (Eds.), *Climate change 2022: Impacts, adaptation and vulnerability. Contribution of Working Group II to the Sixth Assessment Report of the Intergovernmental Panel on Climate Change* (pp. 379–550). Cambridge University Press. https://doi.org/10.1017/9781009325844.005

Cox, J. C., Ross, S. A., & Rubinstein, M. (1979). Option pricing: A simplified approach. *Journal of Financial Economics*, *7*(3), 229–263. https://doi.org/10.1016/0304-405x(79)90015-1

Daniel, K. D., Litterman, R. B., & Wagner, G. (2019). Declining CO_2 price paths. *Proceedings of the National Academy of Sciences*, *116*(42), 20886–20891. https://doi.org/10.1073/pnas.1817444116

Dittes, B., Špačková, O., & Straub, D. (2018). Managing uncertainty in design flood magnitude: Flexible protection strategies versus safety factors. *Journal of Flood Risk Management*, *12*(2), e12455. https://doi.org/10.1111/jfr3.12455

Dittrich, R., Butler, A., Ball, T., Wreford, A., & Moran, D. (2019). Making real options analysis more accessible for climate change adaptation. An application to afforestation as a flood management measure in the Scottish borders. *Journal of Environmental Management*, *245*, 338–347. https://doi.org/10.1016/j.jenvman.2019.05.077

Edwards, T. L., Nowicki, S., Marzeion, B., Hock, R., Goelzer, H., Seroussi, H., et al. (2021). Projected land ice contributions to twenty-first-century sea level rise. *Nature*, *593*(7857), 74–82. https://doi.org/10.1038/s41586-021-03302-y

Erfani, T., Pachos, K., & Harou, J. J. (2018). Real-options water supply planning: Multistage scenario trees for adaptive and flexible capacity expansion under probabilistic climate change uncertainty. *Water Resources Research*, *54*(7), 5069–5087. https://doi.org/10.1029/2017wr021803

Fletcher, S., Lickley, M., & Strzepek, K. (2019). Learning about climate change uncertainty enables flexible water infrastructure planning. *Nature Communications*, *10*(1). https://doi.org/10.1038/s41467-019-09677-x

Fletcher, S., Strzepek, K., Alsaati, A., & de Weck, O. (2019). Learning and flexibility for water supply infrastructure planning under groundwater resource uncertainty. *Environmental Research Letters*, *14*(11), 114022. https://doi.org/10.1088/1748-9326/ab4664

Fox-Kemper, B., Hewitt, H. T., Xiao, C., Aalgeirsdóttir, G., Drijfhout, S. S., Edwards, T. L., et al. (2021). Ocean, cryosphere and sea level change. In V. Masson-Delmotte, P. Zhai, A. Pirani, S. L. Connors, C. Péan, S. Berger, et al. (Eds.), *Climate change 2021: The physical science*

basis. Contribution of Working Group I to the Sixth Assessment Report of the Intergovernmental Panel on Climate Change (pp. 1211–1362). Cambridge University Press. https://doi.org/10.1017/9781009157896.011

Garner, G. G., Hermans, T., Kopp, R. E., Slangen, A. B. A., Edwards, T. L., Levermann, A., et al. (2021a). IPCC AR6 sea-level rise projections [Dataset]. Retrieved from https://podaac.jpl.nasa.gov/announcements/2021-08-09-sea-level-projections-from-the-ipcc-6th-assessment-report

Garner, G. G., Kopp, R. E., Hermans, T., Slangen, A. B. A., Koubbe, G., Turilli, M., et al. (2021b). Framework for Assessing Changes To Sea-Level (FACTS). *Geoscientific Model Development*.

Gersonius, B., Ashley, R., Pathirana, A., & Zevenbergen, C. (2013). Climate change uncertainty: Building flexibility into water and flood risk infrastructure. *Climatic Change*, *116*(2), 411–423. https://doi.org/10.1007/s10584-012-0494-5

Gersonius, B., Morselt, T., van Nieuwenhuijzen, L., Ashley, R., & Zevenbergen, C. (2012). How the failure to account for flexibility in the economic analysis of flood risk and coastal management strategies can result in maladaptive decisions. *Journal of Waterway, Port, Coastal, and Ocean Engineering*, *138*(5), 386–393. https://doi.org/10.1061/(asce)ww.1943-5460.0000142

Guillerminet, M.-L., & Tol, R. S. J. (2008). Decision making under catastrophic risk and learning: The case of the possible collapse of the west Antarctic ice sheet. *Climatic Change*, *91*(1–2), 193–209. https://doi.org/10.1007/s10584-008-9447-4

Guthrie, G. (2019). Real options analysis of climate-change adaptation: Investment flexibility and extreme weather events. *Climatic Change*, *156*(1–2), 231–253. https://doi.org/10.1007/s10584-019-02529-z

Haasnoot, M., Kwakkel, J. H., Walker, W. E., & ter Maat, J. (2013). Dynamic adaptive policy pathways: A method for crafting robust decisions for a deeply uncertain world. *Global Environmental Change*, *23*(2), 485–498. https://doi.org/10.1016/j.gloenvcha.2012.12.006

Haasnoot, M., Middelkoop, H., Offermans, A., van Beek, E., & van Deursen, W. P. A. (2012). Exploring pathways for sustainable water management in river deltas in a changing environment. *Climatic Change*, *115*(3–4), 795–819. https://doi.org/10.1007/s10584-012-0444-2

Haasnoot, M., van 't Klooster, S., & van Alphen, J. (2018). Designing a monitoring system to detect signals to adapt to uncertain climate change. *Global Environmental Change*, *52*, 273–285. https://doi.org/10.1016/j.gloenvcha.2018.08.003

Helgeson, C. (2018). Structuring decisions under deep uncertainty. *Topoi*, *39*(2), 257–269. https://doi.org/10.1007/s11245-018-9584-y

Herman, J. D., Quinn, J. D., Steinschneider, S., Giuliani, M., & Fletcher, S. (2020). Climate adaptation as a control problem: Review and perspectives on dynamic water resources planning under uncertainty. *Water Resources Research*, *56*(2). https://doi.org/10.1029/2019wr025502

Hinkel, J., Church, J. A., Gregory, J. M., Lambert, E., Cozannet, G. L., Lowe, J., et al. (2019). Meeting user needs for sea level rise information: A decision analysis perspective. *Earth's Future*, *7*(3), 320–337. https://doi.org/10.1029/2018ef001071

Hinkel, J., Jaeger, C., Nicholls, R. J., Lowe, J., Renn, O., & Peijun, S. (2015). Sea-level rise scenarios and coastal risk management. *Nature Climate Change*, *5*(3), 188–190. https://doi.org/10.1038/nclimate2505

Hino, M., & Hall, J. W. (2017). Real options analysis of adaptation to changing flood risk: Structural and nonstructural measures. *ASCE-ASME Journal of Risk and Uncertainty in Engineering Systems, Part A: Civil Engineering*, *3*(3), 04017005. https://doi.org/10.1061/ajrua6.0000905

Hui, R., Herman, J., Lund, J., & Madani, K. (2018). Adaptive water infrastructure planning for nonstationary hydrology. *Advances in Water Resources*, *118*, 83–94. https://doi.org/10.1016/j.advwatres.2018.05.009

IPCC. (2021). *Climate change 2021: The physical science basis. Contribution of Working Group I to the Sixth Assessment Report of the Intergovernmental Panel on Climate Change*. Cambridge University Press. https://doi.org/10.1017/9781009157896

Jarrow, R. A., & Rudd, A. (1983). Option pricing.

Jeuland, M., & Whittington, D. (2014). Water resources planning under climate change: Assessing the robustness of real options for the Blue Nile. *Water Resources Research*, *50*(3), 2086–2107. https://doi.org/10.1002/2013wr013705

Kim, K., Ha, S., & Kim, H. (2017). Using real options for urban infrastructure adaptation under climate change. *Journal of Cleaner Production*, *143*, 40–50. https://doi.org/10.1016/j.jclepro.2016.12.152

Kim, M.-J., Nicholls, R. J., Preston, J. M., & Almeida, G. A. M. (2019). An assessment of the optimum timing of coastal flood adaptation given sea-level rise using real options analysis. *Journal of Flood Risk Management*, *12*(S2). https://doi.org/10.1111/jfr3.12494

Kind, J. M., Baayen, J. H., & Botzen, W. J. W. (2018). Benefits and limitations of real options analysis for the practice of river flood risk management. *Water Resources Research*, *54*(4), 3018–3036. https://doi.org/10.1002/2017wr022402

Kolouri, S., Park, S. R., Thorpe, M., Slepcev, D., & Rohde, G. K. (2017). Optimal mass transport: Signal processing and machine-learning applications. *IEEE Signal Processing Magazine*, *34*(4), 43–59. https://doi.org/10.1109/msp.2017.2695801

Kontogianni, A., Tourkolias, C., Damigos, D., & Skourtos, M. (2014). Assessing sea level rise costs and adaptation benefits under uncertainty in Greece. *Environmental Science & Policy*, *37*, 61–78. https://doi.org/10.1016/j.envsci.2013.08.006

Kopp, R., Garner, G. G., Hermans, T. H. J., Jha, S., Kumar, P., Slangen, A. B. A., et al. (2023). The Framework for Assessing Changes To Sea-Level (FACTS) v1.0-rc: A platform for characterizing parametric and structural uncertainty in future global, relative, and extreme sea-level change. https://doi.org/10.5194/egusphere-2023-14

Kopp, R., Oppenheimer, M., O'Reilly, J. L., Drijfhout, S. S., Edwards, T. L., Fox-Kemper, B., et al. (2022). Communicating projection uncertainty and ambiguity in sea-level assessment. https://doi.org/10.1002/essoar.10511663.1

Kwakkel, J. H. (2020). Is real options analysis fit for purpose in supporting climate adaptation planning and decision-making? *WIREs Climate Change*, *11*(3). https://doi.org/10.1002/wcc.638

Lawrence, J., Bell, R., & Stroombergen, A. (2019). A hybrid process to address uncertainty and changing climate risk in coastal areas using dynamic adaptive pathways planning, multi-criteria decision analysis & real options analysis: A New Zealand application. *Sustainability*, *11*(2), 406. https://doi.org/10.3390/su11020406

Levina, E., & Bickel, P. (2001). The earth mover's distance is the Mallows distance: Some insights from statistics. In *Proceedings Eighth IEEE International Conference on Computer Vision. ICCV 2001*. IEEE Computer Society. https://doi.org/10.1109/iccv.2001.937632

Linquiti, P., & Vonortas, N. (2012). The value of flexibility in adapting to climate change: A real options analysis of investments in coastal defense. *Climate Change Economics*, *3*(02), 1250008. https://doi.org/10.1142/s201000781250008x

Liu, H., Wang, Y., Zhang, C., Chen, A. S., & Fu, G. (2018). Assessing real options in urban surface water flood risk management under climate change. *Natural Hazards*, *94*(1), 1–18. https://doi.org/10.1007/s11069-018-3349-1

Martello, M. V., & Whittle, A. J. (2023). Discount rate selection for investments in climate change adaptation and flood risk reduction projects. *Journal of Management in Engineering*, *39*(4). https://doi.org/10.1061/jmenea.meeng-5401

New, M., Reckien, D., Viner, D., Adler, C., Cheong, S.-M., Conde, C., et al. (2022). Decision making options for managing risk. In H.-O. Pörtner, D. C. Roberts, M. Tignor, E. S. Poloczanska, K. Mintenbeck, A. Alegría, et al. (Eds.), *Climate change 2022: Impacts, adaptation, and vulnerability. Contribution of Working Group II to the Sixth Assessment Report of the Intergovernmental Panel on Climate Change* (pp. 2539–2654). Cambridge University Press. https://doi.org/10.1017/9781009325844.026

Oh, S., Kim, K., & Kim, H. (2018). Investment decision for coastal urban development projects considering the impact of climate change: Case study of the Great Garuda Project in Indonesia. *Journal of Cleaner Production*, *178*, 507–514. https://doi.org/10.1016/j.jclepro.2017.12.283

Oppenheimer, M., Glavovic, B., Hinkel, J., van de Wal, R., Magnan, A. K., Abd-Elgawad, A., et al. (2019). Sea level rise and implications for low lying islands, coasts and communities. In H.-O. Pörtner, D. C. Roberts, V. Masson-Delmotte, P. Zhai, M. Tignor, E. Poloczanska, et al. (Eds.), *IPCC Special Report on the Ocean and Cryosphere in a Changing Climate*.

Park, T., Kim, C., & Kim, H. (2013). Valuation of drainage infrastructure improvement under climate change using real options. *Water Resources Management*, *28*(2), 445–457. https://doi.org/10.1007/s11269-013-0492-z

Ryu, Y., Kim, Y.-O., Seo, S. B., & Seo, I. W. (2018). Application of real option analysis for planning under climate change uncertainty: A case study for evaluation of flood mitigation plans in Korea. *Mitigation and Adaptation Strategies for Global Change*, *23*(6), 803–819. https://doi.org/10.1007/s11027-017-9760-1

Scambos, T., Bell, R., Alley, R., Anandakrishnan, S., Bromwich, D., Brunt, K., et al. (2017). How much, how fast?: A science review and outlook for research on the instability of Antarctica's Thwaites Glacier in the 21st century. *Global and Planetary Change*, *153*, 16–34. https://doi.org/10.1016/j.gloplacha.2017.04.008

Schou, E., Thorsen, B. J., & Jacobsen, J. B. (2015). Regeneration decisions in forestry under climate change related uncertainties and risks: Effects of three different aspects of uncertainty. *Forest Policy and Economics*, *50*, 11–19. https://doi.org/10.1016/j.forpol.2014.09.006

Sims, C., Null, S. E., Medellin-Azuara, J., & Odame, A. (2021). Hurry up or wait: Are private investments in climate change delayed? *Climate Change Economics*, *12*(4). https://doi.org/10.1142/s2010007821500123

Slangen, A. B. A., Haasnoot, M., & Winter, G. (2022). Rethinking sea-level projections using families and timing differences. *Earth's Future*, *10*(4). https://doi.org/10.1029/2021ef002576

van der Pol, T. D., & Hinkel, J. (2019). Uncertainty representations of mean sea-level change: A telephone game? *Climatic Change*, *152*(3–4), 393–411. https://doi.org/10.1007/s10584-018-2359-z

van der Pol, T. D., Hinkel, J., Merkens, J., MacPherson, L., Vafeidis, A. T., Arns, A., & Dangendorf, S. (2021). Regional economic analysis of flood defence heights at the German Baltic Sea coast: A multi-method cost-benefit approach for flood prevention. *Climate Risk Management*, *32*, 100289. https://doi.org/10.1016/j.crm.2021.100289

van der Pol, T. D., van Ierland, E. C., & Gabbert, S. (2015). Economic analysis of adaptive strategies for flood risk management under climate change. *Mitigation and Adaptation Strategies for Global Change*, *22*(2), 267–285. https://doi.org/10.1007/s11027-015-9637-0

van der Pol, T. D., van Ierland, E., & Weikard, H.-P. (2013). Optimal dike investments under uncertainty and learning about increasing water levels. *Journal of Flood Risk Management*, *7*(4), 308–318. https://doi.org/10.1111/jfr3.12063

Völz, V., & Hinkel, J. (2023a). Climate learning scenarios for adaptation decision analyses: Review and classification. *Climate Risk Management*, *40*, 100512. https://doi.org/10.1016/j.crm.2023.100512

Völz, V., & Hinkel, J. (2023b). Sea level rise learning scenarios for adaptive decision-making based on IPCC AR6. *Zenodo*. https://doi.org/10.5281/zenodo.8079469

Walker, W. E., Rahman, S., & Cave, J. (2001). Adaptive policies, policy analysis, and policy-making. *European Journal of Operational Research*, *128*(2), 282–289. https://doi.org/10.1016/s0377-2217(00)00071-0

Weaver, C. P., Moss, R. H., Ebi, K. L., Gleick, P. H., Stern, P. C., Tebaldi, C., et al. (2017). Corrigendum: 'Reframing climate change assessments around risk: Recommendations for the US National Climate Assessment' (2017 Environ. Res. Lett. 12 080201). *Environmental Research Letters*, *12*(9), 099501. https://doi.org/10.1088/1748-9326/aa846a

Webster, M., Jakobovits, L., & Norton, J. (2008). Learning about climate change and implications for near-term policy. *Climatic Change*, *89*(1–2), 67–85. https://doi.org/10.1007/s10584-008-9406-0

Woodward, M., Kapelan, Z., & Gouldby, B. (2014). Adaptive flood risk management under climate change uncertainty using real options and optimization. *Risk Analysis*, *34*(1), 75–92. https://doi.org/10.1111/risa.12088

Wreford, A., Dittrich, R., & Pol, T. D. (2020). The added value of real options analysis for climate change adaptation. *WIREs Climate Change*, *11*(3). https://doi.org/10.1002/wcc.642